Prepared for submission to JCAP

Probing the neutrino mass hierarchy with the rise time of a supernova burst

Sovan Chakraborty,[a] **Tobias Fischer,**[b,c] **Lorenz Hüdepohl,**[d] **Hans-Thomas Janka,**[d] **Alessandro Mirizzi,**[a] **Pasquale D. Serpico.**[e]

[a]II Institut für Theoretische Physik, Universität Hamburg, Luruper Chaussee 149, 22761 Hamburg, Germany

[b]GSI, Helmholtzzentrum für Schwerionenforschung GmbH, Planckstr. 1, 64291 Darmstadt, Germany

[c]Technische Universität Darmstadt, Schlossgartenstr. 9, 64289 Darmstadt, Germany

[d]Max-Planck-Institut für Astrophysik, Karl-Schwarzschild-Str. 1, 85748 Garching, Germany

[e]LAPTh, UMR 5108, 9 chemin de Bellevue–BP 110, 74941 Annecy-Le-Vieux, France

Abstract. The rise time of a Galactic supernova (SN) $\overline{\nu}_e$ lightcurve, observable at a high-statistics experiment such as the Icecube Cherenkov detector, can provide a diagnostic tool for the neutrino mass hierarchy at "large" 1-3 leptonic mixing angle θ_{13}. Thanks to the interplay of matter suppression of collective effects at early postbounce times on one hand and the presence of the ordinary Mikheyev-Smirnov-Wolfenstein effect in the outer layers of the SN on the other hand, a sufficiently fast rise time and the lack of long accretion-enhancement of the early iron-core SN signal are indicative of an inverted mass hierarchy. We investigate results from an extensive set of stellar core-collapse simulations obtained with two different codes to explore the robustness of these features concerning differences of the progenitor structure, high-density equation of state, detailed treatment of neutrino-matter interactions, and dimensionality of the simulation. We find that the faster rise time for an inverted hierarchy as compared to normal hierarchy is predicted by all models, yielding a promising perspective for the detection of this signature from a future Galactic SN event.

Keywords: Neutrino mass and mixing, supernovae

Contents

1 Introduction

The detection of neutrinos from core-collapse supernovae (SNe) represents the most exciting frontier of low-energy neutrino (ν) astronomy. Even though galactic SNe are rare, perhaps a few per century, the existing large underground neutrino detectors and the numerous planned ones increase the confidence that a high-statistics SN neutrino signal will be eventually observed. Such a detection would provide a plethora of astrophysical information on the SN explosion mechanism, and could offer a handle on particle physics such as ν masses and mixings, too (see, e.g., [1]).

In particular, the flavor conversions occurring deep inside the star could leave an imprint on the observable SN neutrino burst. A lot of attention has been payed to possible signatures of the Mikheyev-Smirnov-Wolfenstein (MSW) effect [2, 3] with the ordinary matter in the stellar envelope [4]. Moreover, in recent years it has been realized that in the deepest supernova regions the neutrino density is so high that the neutrino-neutrino interactions [5, 6] dominate the flavor evolution in a highly non-trivial way (for a review see [7]). The general result of these studies is that rapid conversions between different flavors are possible and can occur collectively, i.e. in a coherent fashion for many modes over large energy ranges. Unfortunately, the occurrence of these effects is strongly dependent on the original SN emission features, which makes a *general* characterization of the observable SN neutrino spectra at Earth in terms of the original ones a formidable task (see, e.g, [8–13]). At the moment we are still far from a complete understanding of this complex flavor-dynamics.

However, *the lack of a complete understanding* should not be confused with *a complete lack of understanding*. In fact, for some conditions/regimes a relatively robust comprehension has been achieved. This is *not* the case, unfortunately, for the long-time cooling phase (post-bounce time $t_{\rm p.b.} \gtrsim 1$ s). In principle, rich time- and energy-dependent collective dynamics may be present there [11–14], on the top of which peculiar time-dependent modification of the flavor content of the flux could be induced by MSW effects associated to the shock-wave propagation in the stellar envelope [15–19]. Since our current understanding suggests that the resulting neutrino spectra depend on many poorly understood details, sharp predictions for the flavor evolution are very challenging if not impossible at present. Furthermore, during the cooling phase all neutrino flavors originate close to the neutron star surface, where the

material is very neutron rich, suppressing charged-current reactions for $\overline{\nu}_e$. Therefore, one expects that the luminosities and spectra of $\overline{\nu}_e$ and $\overline{\nu}_x$ become quite similar, making it much harder to see flavor oscillation effects at all in the dominant $\overline{\nu}_e$ channel, which is currently the optimal one. This is due to the fact that all large existing and near-future detectors primarily see inverse beta decay events $\overline{\nu}_e + p \to n + e^+$. The relative similarity of $\overline{\nu}_e$ and $\overline{\nu}_x$ spectra seems to be in fact qualitatively confirmed by recent 1D long-time simulations [20, 21].

In order to direct future searches and experimental perspectives, a more robust strategy is to focus on the early phase of the SN neutrino signal, in a time window where relatively robust expectations exist for the neutrino emission spectra and for the flavor dynamics. The largest difference among the flavor fluxes arises during the first 10–20 ms after bounce when the outer layers of the collapsed core deleptonize, leading to the prompt ν_e burst. Since negligible $\bar{\nu}_e$ and ν_x fluxes are emitted during this phase, self-induced oscillations are simply absent: collective effects do not give rise to any flavor transformation during the neutronization burst [22]. [1] Additionally, at these early times, since the shock wave stalls at low radii close to the neutrinosphere, the MSW flavor transitions occurring at larger radii would essentially probe the static SN progenitor profile. In this situation, the characterization of the flavor conversions is straightforward and, since the model predictions for the energy and luminosity of the burst are fairly robust, the observation of the burst gives direct information about the survival probability of ν_e and then on the mixing parameters [25]. Indeed, a strong suppression of the ν_e burst would be a smoking gun for the normal neutrino mass hierarchy (NH: $\Delta m^2_{\rm atm} = m^2_3 - m^2_{1,2} > 0$) in the case of a "large" $1-3$ leptonic mixing angle (i.e. $\sin^2\theta_{13} \gtrsim 10^{-3}$), as currently suggested by the long-baseline $\nu_\mu \to \nu_e$ experiments [26, 27], especially when analysed in combination with other oscillation data [28, 29]. However, with current "$\overline{\nu}_e$ SN detectors", such effects are challenging-to-impossible to detect, and one has to invoke future Mton-class water Cherenkov detectors [25] or large liquid-argon time projection chambers [30], to achieve enough sensitivity to these ν_e signal features.

On the other hand, the subsequent phase of mass accretion, characterized by postbounce times $t_{\rm p.b.}$ of up to a few hundreds of ms, represents a particularly interesting possibility for detecting signatures of flavor transformations also in the accessible $\overline{\nu}_e$ channel (see [31] for a discussion in the context of SN1987A). First of all, one can more easily afford to simulate these early stages with sufficiently realistic neutrino transport than the longer timescales of later cooling phases. Also, the neutrino signal properties are largely independent of the detailed mechanism of the explosion (and actually of the question whether an explosion takes place at all), since the revival of the shock wave has yet to take place. All modern simulations available indicate that the neutrino fluxes as well as the flavor-dependent flux differences are large in this phase, with a robust hierarchy for the neutrino number fluxes, $F_{\nu_e} > F_{\overline{\nu}_e} \gg F_{\nu_x}$, where ν_x indicates the non-electron flavors. Moreover, it has been recently realized [32, 33] that the net electron densities n_e reached above the neutrinosphere in realistic SN models exceed the neutrino density n_ν, significantly suppressing the development of the self-induced neutrino oscillations according to the "multi-angle matter suppression" mechanism first described in [34]. The matter suppression ranges from complete (when $n_e \gg n_\nu$) to partial (when $n_e \gtrsim n_\nu$), producing in principle intriguing time-dependent features. Using as benchmark the results of the hydrodynamical SN simulations of the Basel/Darmstadt group for different iron-core SN models [20], Ref. [33] found complete matter suppression for post-

[1] An exception is constituted by the case of low-mass SNe with an oxygen-neon-magnesium core, where the matter density profile can be so steep that the usual MSW matter effects occur within the region of high neutrino densities close to the neutrino sphere, triggering self-induced flavor conversions there [23, 24].

bounce times $t_{\rm p.b.} \lesssim 0.2$ s, and partial flavor conversions for $0.2 \lesssim t_{\rm p.b.} \lesssim 0.4$ s. This result has been independently confirmed in Ref. [35]. More recently, in a work based on a iron-core SN model from the Garching group complete matter suppression has been found for all the duration of the accretion phase [36]. When the matter suppression is complete, the ν signal will be processed only by the usual MSW effect in the SN mantle with the static progenitor profile. In this situation, the characterization of the SN neutrino signal results is straightforward [4]. Moreover, in the presence of a "large" θ_{13} mixing angle one would expect significant differences in the observable $\overline{\nu}_e$ flux for the two mass hierarchies [4].

Motivated by these considerations, we devote our work to a first characterization of the early SN neutrino lightcurve signal in the largest current neutrino detector for such a purpose, namely the IceCube Cherenkov detector in the ice at the South Pole. We shall focus in particular on observables sensitive to the neutrino mass hierarchy. The plan of our work is as follows. In Sec. 2 we present the input neutrino flux models we considered, obtained from recent radiation-hydrodynamical simulations from the Basel/Darmstadt [20] and Garching [37] groups. In Sec. 3 we characterize the neutrino flavor conversions during the accretion phase. In Section 4 we describe the supernova neutrino signal in IceCube. We show how the analysis of the neutrino lightcurve during the accretion phase may be a powerful tool to probe the neutrino emission features and the mass hierarchy in the likely case the mixing angle θ_{13} is not too small. In order to investigate the robustness of our result, we provide an extensive scan of several simulations from the two different groups, finding similar features in all the cases we analyzed. Finally, in Sec. 5 we discuss future perspectives and we conclude.

2 Numerical models for supernova neutrino emission

We summarize here the main aspects of the different SN models considered for the present investigation. These are simulations that were performed by the two different supernova groups from Basel/Darmstadt and Garching. In Sec. 2.2 a qualitative description of the features and some differences found in two representative SN simulations from these groups is given. Readers not interested in details may skip directly to Sec. 2.3, where the basic input and parametrizations used in the following analysis are summarized.

2.1 Supernova models considered

The Basel/Darmstadt simulations were performed using the SN code AGILE-BOLTZTRAN. It is based on general relativistic radiation hydrodynamics and three-flavor Boltzmann neutrino transport in spherical symmetry (for details of the SN modeling, see [40]). The simulations we deal with here used the set of opacities following Ref. [41] and in addition nucleon-nucleon-bremsstrahlung [42]. For the present analysis, the equation of state for hot and dense nuclear matter from Shen et al. [43] was used. Several different progenitors will be considered, based on the study in Ref. [20]. Supernova progenitors with iron cores have extended, high-density Si-layers surrounding the central iron core. Therefore the postbounce evolution leads to a long accretion phase that can last for several hundreds of milliseconds (depending on the progenitor). Because neutrino-driven explosions cannot be obtained in spherically symmetric SN models for iron-core progenitors, the charged-current rates were enhanced in the gain region during the postbounce accretion phase in order to trigger explosions. The increased energy deposition leads to explosions for the 10.8 and 18 $M_\odot$ progenitors [38] considered here (for details, see [20]). The postbounce times for the onset of explosion are about 320 ms for both models. In addition, we simulated the 15 $M_\odot$ progenitor model from the

same series of Ref. [38] using the same physics input as in Ref. [20]. The resulting evolution is in qualitative agreement with the previous simulations of the 10.8 and 18 $M_\odot$.

The Garching models [37] were computed with the PROMETHEUS-VERTEX code [44, 45]. It contains hydrodynamics modules for both spherically symmetric (1D) and multi-dimensional simulations (using a polar coordinate grid). These are based on a conservative and explicit Eulerian implementation of a Godunov-type scheme with higher-order spatial and temporal accuracy. Although the solver is Newtonian, it employs a correction to the gravitational potential approximating effects of general relativistic gravity (case A of Ref. [46]). The module for the energy-dependent, three-flavor neutrino transport solves the $\mathcal{O}(v/c)$ moment equations for neutrino energy, momentum, and lepton number with a variable Eddington-factor closure obtained from a model-Boltzmann equation. General relativistic redshifting is included and a "ray-by-ray plus" approximation is employed for treating multi-dimensional problems. The set of neutrino processes used for the simulations analyzed in the present work was discussed in Ref. [45] (see Appendix A there). It is supplemented by the improved electron-capture rates on heavy nuclei of Ref. [47] and the inelastic neutrino-nucleus scattering rates of Ref. [48], both of which have some influence on the details of the core-infall phase before bounce and on the exact formation point of the supernova shock.

The set of spherically symmetric core-collapse simulations from the Garching group is based on a selection of progenitor models from Ref. [38] in addition to the older 15 $M_\odot$ model from Ref. [49], for which we also evaluate results of an axially-symmetric (2D) simulation published in Ref. [50]. All calculations were performed with the equation of state of Lattimer & Swesty [51]. None of the runs produced an explosion within the evolution periods considered for the present work.

2.2 Neutrino emission properties

Here we concentrate on the early postbounce evolution, where according to the current understanding non-radial hydrodynamic flows, if present, do not have a very strong influence on the properties of the neutrino radiation leaving the supernova core.

Figure 1 illustrates the evolution of the neutrino luminosities, average energies $\langle E_\nu \rangle$ and energy-shape parameter α for ν_e, $\overline{\nu}_e$ and $\overline{\nu}_x$, sampled in the observer frame at infinity (for a definition of these observables, see [52]). Here, ν_x indicates both (μ, τ)-(anti)neutrinos. The neutrino emission properties observed at infinity are determined at the moment of decoupling, which defines the neutrino-energy and flavor dependent spheres of last scattering [53]. The neutrinos which contribute to the luminosity at infinity carry information about the state of the matter at the moment of decoupling. The energy-shape parameter α is defined as [53, 55]

$$\alpha = \frac{2\langle E_\nu \rangle^2 - \langle E_\nu^2 \rangle}{\langle E_\nu^2 \rangle - \langle E_\nu \rangle^2}\,, \tag{2.1}$$

i.e. it is a dimensionless parameter containing information on the second moment of the distribution, $\langle E_\nu^2 \rangle$. In the following, we will discuss general properties of the observables shown in Fig. 1.

During the early postbounce accretion phase all investigated supernova models have a common feature, which they also share with results published in Refs. [20, 40, 50, 52, 54]: The luminosity of heavy-lepton neutrinos and antineutrinos (henceforth collectively denoted by ν_x) rises initially faster than that of electron antineutrinos $\overline{\nu}_e$. Note that $\overline{\nu}_e$ and ν_x in contrast to ν_e are not emitted in any significant amounts during the core-collapse phase until core bounce. Instead, their vivid production sets in only when the bounce shock starts to

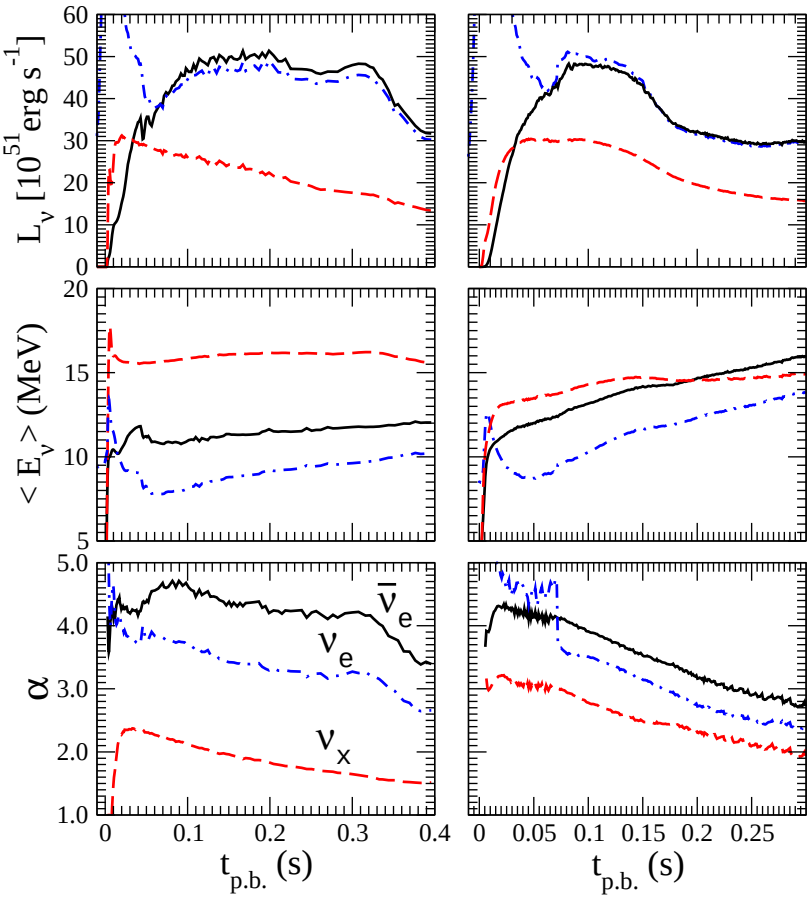

Figure 1. Early postbounce evolution of luminosities (top panels), mean energies (middle panels) and α-fit parameters (bottom panels), comparing two selected simulations from the Basel/Darmstadt group [20] using the 15 $M_\odot$ progenitor from Ref. [38] (left plots), and from the Garching group [37] using the 15 $M_\odot$ progenitor from Ref. [49] (right plots). Note that ν_x means either $\nu_{\mu,\tau}$ or $\overline{\nu}_{\mu,\tau}$ and the corresponding luminosity is for one of these species.

heat swept-up material to high temperatures. This allows nucleon-nucleon bremsstrahlung to become efficient and positrons to appear so that electron-positron annihilation can also take place. These processes become more and more important as the temperature rises and the electron degeneracy drops as a consequence of the deleptonization triggered by the prompt ν_e burst. The production of $\overline{\nu}_e$ is more strongly suppressed than that of ν_x during the first $\sim$20 ms after bounce because of the high degeneracy of electrons and ν_e, which are present in very large numbers before and during the emission of the deleptonization burst[2].

The steep initial increase of the ν_x luminosity is followed by a relatively abrupt termination of this growth at a value of typically a few 10^{52} erg/s (for a single kind of heavy-lepton neutrino), considerably (roughly a factor of two) below the peak luminosity reached by $\overline{\nu}_e$ more gradually about 0.1 s later. The ν_e and $\overline{\nu}_e$ luminosities then attain a roughly constant plateau level, during which the emission of these neutrinos is enhanced by their highly efficient

[2]Because the high electron degeneracy allows only for a low abundance of positrons, the production of $\overline{\nu}_e$ by e^+e^- annihilation and e^+ captures on neutrons is not efficient. Moreover, since in the optically thick regime ν_e are in chemical equilibrium with the matter their degeneracy also blocks the phase space for the creation of $\overline{\nu}_e$ via nucleon-nucleon bremsstrahlung.

production via charged-current processes (electron and positron captures on free nucleons) in the matter that forms a thick, hot mantle around the newly born proto-neutron star after having been accreted through the standing bounce shock. The duration of this plateau phase depends on the core structure of the collapsing star and the corresponding shallow decline of the mass-infall rate with time. It varies with the progenitor. A faster luminosity drop sets in when the density and thus mass accretion rate decreases more abruptly. This can be associated with, e.g., the infall of an interface between progenitor shells containing different chemical compositions or with the onset of the explosion, which quenches further accretion. Note that explosions were induced artificially for the massive iron-core progenitors from the Basel/Darmstadt group. The oscillatory behavior of the electron-flavor luminosities shown in Fig. 1 (left panel) reflects the back- and forward propagating bounce shock, which in turn leads to an oscillating mass-accretion rate behind the supernova shock.

While the production of ν_e and $\overline{\nu}_e$ in the hot accretion layer is very important, heavy-lepton neutrinos are created exclusively by neutral-current pair processes, i.e., nucleon-nucleon bremsstrahlung as well as electron-positron and ν_e-$\overline{\nu}_e$ pair annihilation. (Note that the last process is included only in the Garching models.) Consequently, heavy-lepton neutrinos are thermally less strongly coupled to the stellar medium. Their main production occurs deeper inside the newly born proto-neutron star and additional contributions from the accretion layer are less significant. Therefore ν_x escape effectively from a layer with smaller radiating surface and their luminosity remains lower than that of electron-flavor neutrinos (since the emission is approximately blackbody-like, the luminosity L_ν scales with the neutrinosphere radius R_ν and temperature T_ν roughly like $L_\nu \propto R_\nu^2 T_\nu^4$). The temporal evolution of the ν_x luminosity after the peak depends on two factors, which in combination have a complex influence on the evolution of temperature and radius of the corresponding neutrinosphere: (a) the contraction behavior of the core of the nascent proto-neutron star and (b) the growing thickness of the surrounding accretion layer in response to the continuous infall of matter from the collapsing progenitor star. On the one hand a more massive accretion layer compresses the proto-neutron star core but at the same time leads to higher temperatures, therefore not only enhancing the ν_e and $\overline{\nu}_e$ emission but also the ν_x luminosity of more massive progenitors. On the other hand the core contracts faster also for a softer nuclear equation of state. Therefore, both the different stellar progenitors (with a different structure of their iron core and surrounding regions) and the different equations of state have important consequences for the properties and evolution of the emission of neutrinos and antineutrinos of all flavors during the postbounce accretion phase. At least part of the differences between luminosities and mean energies from simulations of the Basel/Darmstadt and Garching groups shown in Fig. 1 can be explained by the different equations of state and progenitors used in these simulations.

It is important to note that outside the radius where pair-production processes have essentially ceased (at the so-called "energy-sphere"), ν_x still diffuse through an overlying layer of opaque matter, in which they scatter frequently off neutrons and protons before they can escape freely at their "transport-sphere". Although the energy transfers from high-energy ν_x to the nucleons of the cooler environment by individual scatterings are small, the cumulative effect of many scattering reactions adds up to a noticeable down-grading in energy space of ν_x that finally stream off the transport-sphere (for a detailed discussion, see Ref. [55]). The corresponding spectral changes are accounted for in the Garching models because the effects of nucleon recoil and thermal motions (as well as weak-magnetism corrections) are included in the treatment of neutrino-nucleon interactions (see Appendix A of Ref. [45]). They could

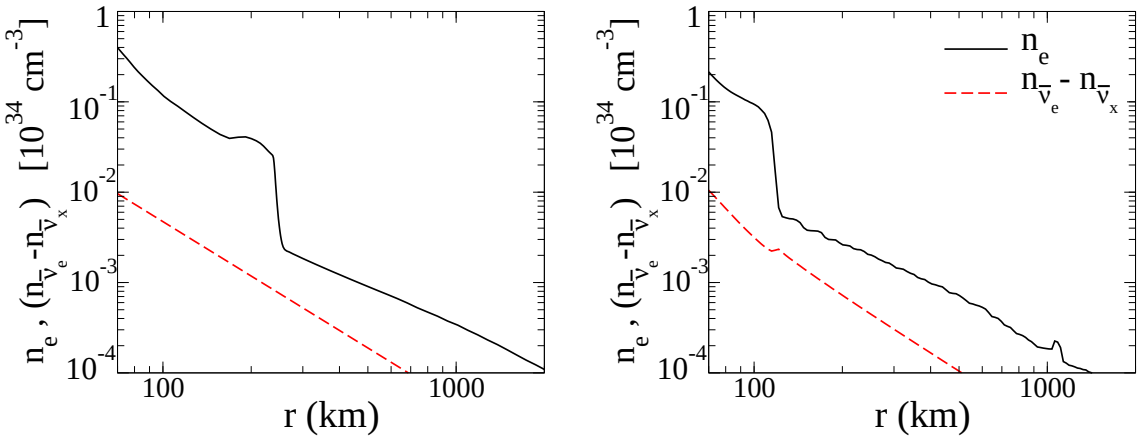

Figure 2. Radial profiles of net-electron density (continuous black curves) and neutrino-density difference $n_{\bar{\nu}_e} - n_{\bar{\nu}_x}$ (dashed red curves) during the early postbounce accretion phase, comparing the Basel/Darmstadt results (left panel) with the Garching results (right panel) at $t_{\rm p.b.}$ =0.125 s.

account for the significantly less energetic heavy-lepton neutrinos obtained in the Garching models compared to the Basel/Darmstadt models (see Fig. 1), where corrections from weak magnetism and nucleon recoil were not taken into account. Note that applying identical input physics to core-collapse supernova simulations, both Basel/Darmstadt and Garching results agree qualitatively and quantitatively [52, 54].

In contrast to the spherically symmetric (1D) case, the observable neutrino luminosities and mean energies predicted by multi-dimensional supernova simulations exhibit short-time variations with considerable amplitudes during the postbounce accretion phase. This is connected to the presence of large-scale asymmetries as a consequence of hydrodynamic instabilities in the layer between proto-neutron star surface and stalled bounce shock. These lead to time-dependent hot spots and anisotropic neutrino production in the cooling region of the settling accretion flow. Such effects were discussed in detail for axially symmetric (2D) models in Refs. [50, 56] and for 3D models in Ref. [57].

In the bottom panels of Fig. 1 we show the time evolution of the spectral parameter α of Eq. (2.1). We remind the reader that a Maxwell-Boltzmann spectrum has $\alpha = 2$. Numerical spectra show values of $\alpha = 2$–4, i.e. the spectra are "pinched". For both supernova models, the ν_x spectrum is less pinched than that of ν_e and $\overline{\nu}_e$. Furthermore, the α parameter for the ν_x spectrum decreases during the accretion phase for both supernova models, but its value is higher (the ν_x spectrum thus more pinched) in the Garching model, where nucleon recoil is included. On the other hand, the α parameter for the ν_e and $\overline{\nu}_e$ spectra is rather constant in the Basel/Darmstadt simulation and decreases with time in the Garching simulation.

In addition to the evolution of luminosities, mean energies, and α's, we show in Fig. 2 radial profiles of the net-electron density and of the neutrino-density difference between $\overline{\nu}_e$ and $\overline{\nu}_x$ (entering the ν equations of motion [32, 33, 36]) at a representative postbounce time comparing again the Basel/Darmstadt (left panel) and Garching models (right panel). The net-electron density is greater than the neutrino-density difference. This result indicates that neutrino-flavor oscillations are matter dominated at early times. In fact, it has been shown recently that collective favor oscillations are suppressed during the postbounce mass accretion phase [32, 33, 36], as we will discuss in Sec. 3. We remind the reader that matter dominance at early postbounce times has recently been found also in the 2D SN simulations

presented in Ref. [58].

2.3 Parameterization of neutrino radiation properties

In summary, numerical simulations of core-collapse supernovae provide the un-oscillated doubly differential neutrino distribution in energy and time,

$$F_\nu^0 \equiv \frac{d^2 N_\nu}{dt\, dE}\,. \tag{2.2}$$

where $\nu = \{\nu_e, \overline{\nu}_e, \overline{\nu}_x\}$ in standard notation [4]. This is related to the *instantaneous* (time-dependent) luminosity via

$$L_\nu = \int_0^\infty dE E F_\nu^0 \ . \tag{2.3}$$

We factorize both the Basel/Darmstadt and the Garching groups' simulation outputs as follows:

$$F_\nu^0 = \frac{dN_\nu}{dt}\varphi(E_\nu) \tag{2.4}$$

for each flavor ($\nu = \nu_e, \overline{\nu}_e, \nu_x$), where

$$\frac{dN_\nu}{dt} = \frac{L_\nu}{\langle E_\nu \rangle} \tag{2.5}$$

represents the neutrino emission rate (number of ν's per unit of time) with mean neutrino energy $\langle E_\nu \rangle$. The function $\varphi(E)$ is the normalized ($\int \varphi(E) dE = 1$) energy spectrum parametrized as in Ref. [53]

$$\varphi(E) = \frac{1}{\langle E_\nu \rangle} \frac{(1+\alpha)^{1+\alpha}}{\Gamma(1+\alpha)} \left(\frac{E}{\langle E_\nu \rangle}\right)^\alpha \exp\left[-(1+\alpha)\frac{E}{\langle E_\nu \rangle}\right] , \tag{2.6}$$

where α is defined in Eq. (2.1). In general, L_ν, $\langle E_\nu \rangle$ and α are all functions of time, and are extracted directly from the simulations at hand.

In the following section we will limit our analysis to $t_{\rm p.b.} \leq 0.2$ s. In this time window of the pre-explosion phase the non-radial mass motions connected to hydrodynamical instabilities (i.e., hot-bubble convection and the standing accretion shock instability) found in multi-dimensional SN models have still to grow to their full strength [57]. Indeed, comparing the neutrino luminosities and mean energies of the 15 $M_\odot$ Garching 1D model of Fig. 1 with the corresponding quantities for the 15 $M_\odot$ Garching 2D model in Fig. 6 and 7 of Ref. [50], one realizes that during the early accretion phase only minor differences arise between these two cases. Therefore, the 1D SN models we will use for our study are sufficient for an accurate characterization of the neutrino signal and of the SN matter density at early postbounce times. We will show this explicitly in Sec. 4 where we will compare our results for 1D and 2D SN models. This similarity between 1D and 2D results also simplifies the neutrino flavor conversion physics, as explained in the following section.

3 Neutrino flavor conversions

The emitted SN neutrino flux is processed by self-induced and MSW oscillation effects during its propagation. The self-induced effects would take place within $r \sim \mathcal{O}(10^3)$ km from the

neutrinosphere whereas the MSW transitions take place at larger radii, in the region $r \sim 10^4$–10^5 km. As the self-induced and MSW effects are widely separated in space, they can be considered independently of each other. In the normal mass hierarchy (NH, $\Delta m^2_{\rm atm} > 0$) and for the spectral ordering of the accretion phase, no self-induced flavor conversion will occur. Instead, in inverted mass hierarchy (IH, $\Delta m^2_{\rm atm} < 0$) potentially large self-induced effects could be expected [12]. However, it has been shown in [32, 33, 36] that the trajectory-dependent multi-angle effects associated with the dense ordinary matter suppress collective oscillations in actual models of iron-core SNe. This is related to the high matter densities during the accretion phase in core-collapse SNe of massive iron-core progenitors. Indeed, when the electron density n_e significantly exceeds the neutrino density n_ν, it was expected that the large trajectory-dependent phase dispersion induced by the matter would suppress the collective phenomena [34]. Depending on the electron density, the matter suppression can be complete, when $n_e \gg n_\nu$, or partial when the matter dominance is less pronounced Finally, when $n_e \approx n_\nu$, the interference of the two comparable effects would lead to the decoherence of the collective neutrino flavor changes, producing an equal mixture between the oscillating electron and non-electron neutrino species [34].

From the comparison in Fig. 2 of the radial evolution of the net electron density n_e (continuous curves) and of neutrino density difference $n_{\bar\nu_e} - n_{\bar\nu_x}$ entering the equations of motion [32, 33, 36] (dashed curves) at $t_{\rm p.b.} = 0.125$ s for the Basel/Darmstadt (left panel) and the Garching (right panel) models presented in Sec. 2, we realize that in both cases the matter density dominates over the neutrino density. It completely suppresses the flavor conversions. In the following we will focus on an early time-window $t_{\rm p.b.} < \mathcal{O}\,(0.2$ s) where the matter density even largely exceeds the neutrino density, and hence also completely suppresses the collective oscillations for the cases under investigation. [3] We remind the reader that the matter suppression of self-induced oscillations during the accretion phase has been explicitly studied in [33] for the 15 $M_\odot$ Basel/Darmstadt model and in [36] for the Garching model, respectively.

In this situation, the neutrino fluxes can only undergo the traditional MSW conversions in SN while passing through the outer layers of the star. Therefore, it is straightforward how to calculate the $\overline{\nu}_e$ flux at Earth in the different cases [4]. In particular, in NH one finds

$$F_{\bar\nu_e} = \cos^2\theta_{12} F^0_{\bar\nu_e} + \sin^2\theta_{12} F^0_{\bar\nu_x} \ , \tag{3.1}$$

where θ_{12} is the 1–2 mixing angle, with $\sin^2\theta_{12} \simeq 0.31$ [28]. In IH for "large" θ_{13} (i.e. with $\sin^2\theta_{13} \gtrsim 10^{-3}$) one gets

$$F_{\bar\nu_e} = F^0_{\bar\nu_x} \ , \tag{3.2}$$

while for "small" θ_{13} (i.e. with $\sin^2\theta_{13} \lesssim 10^{-5}$) one finds

$$F_{\bar\nu_e} = \cos^2\theta_{12} F^0_{\bar\nu_e} + \sin^2\theta_{12} F^0_{\bar\nu_x} \ . \tag{3.3}$$

Then, it is clear that for "large" θ_{13} the $\overline{\nu}_e$ flux at the Earth (in the likely case where it is unshielded by the core) is basically reflecting the original $F_{\bar\nu_x}$ flux, if IH is realized, or closely matching the $F_{\bar\nu_e}$ flux, in case of NH. Since these two extremes show significant qualitative differences (see Fig. 1), one might hope to be able to distinguish these two possibilities. We shall see in the next section that this appears to be a promising perspective for neutrino detections at IceCube.

[3] Note that this is conservative in many respects, e.g. in the model studied in [36] the matter suppression is complete during the entire accretion phase.

4 Neutrino lightcurve in IceCube

The idea of using Gigaton scale high energy ν under-ice detectors as supernova neutrino bservatories was first proposed in [59]. The method is based on a sudden, correlated increase in the photomultiplier count rate on a timescale on the order of 10 s (see Ref. [60] for a recent description).

In its completed configuration and with its data acquisition system, IceCube with its 4800 optical modules, has about 3 Mton effective detection volume, representing the largest current detectors for supernova neutrinos. The SN neutrinos streaming through the antartic ice interact mostly through $\overline{\nu}_e + p \to n + e^+$ reactions [61]. While fine-grained detectors, like Super-Kamiokande, reconstruct individual neutrinos on an event-by-event basis, IceCube only picks up the average Cherenkov glow of the ice. To estimate the detection rate we closely follow Refs. [62, 63]. The only change consists in replacing the product of Eq. (1) and Eq. (6) in [62] with the following rate of energy deposition per proton

$$R_{\overline{\nu}_e} = \int_0^\infty dE\, F_{\overline{\nu}_e}\, E_{\rm rel}(E)\, \sigma(E)\,, \tag{4.1}$$

with $E_{\rm rel}(E)$ being the energy released by a neutrino of energy E.

In Figure 3 we show the expected counting rate in IceCube for a galactic supernova at a distance of $d = 10$ kpc. This "fiducial" distance has been chosen consistently with average distance expectations [64] for different SN models. Since we are interested in the possibility of the mass hierarchy discrimination, we focus on the likely case of a large $\sin^2\theta_{13}$ where the observable $\overline{\nu}_e$ signal would be different in the two hierarchies [see Eqs. (3.1)–(3.2)]. We refer to the cases of 15 $M_\odot$ progenitor masses previously used for illustration, with the left panels referring to the Basel/Darmstadt model and right panels to the Garching one. The NH cases are shown with continuous curves, while the IH cases are the dashed curves. At the bottom panels we have used 2 ms bins with typical Poisson error estimates from the photomultiplier background noise, i.e. 280 $\rm s^{-1}$ in each optical module [63].

For each of the two models, the difference between the observed neutrino lightcurve in the NH vs. IH is evident. For the NH case, a relatively long hump in the signal associated with the accretion is clearly visible (note that in the Basel/Darmstadt case the maximum would be reached after $t_{\rm p.b.} \sim 0.2\,$s, "out of scale"). In the case of IH, the lightcurve has a more sudden rise, followed by a decline. Note that both luminosity behavior and trend of growing energy of $\overline{\nu}_e$ shown in Fig. 1 contribute to the final shape of the curves. In particular, the prominent difference between the Basel/Darmstadt and Garching results in the initial, steep rise of the signal is enhanced by the much higher $\overline{\nu}_x$ energies of the Basel/Darmstadt model. Moreover, for the Basel/Darmstadt model in IH after $t_{\rm p.b.}$= 0.01 s one finds a monotonically decreasing signal that reflects the decline of the $\overline{\nu}_x$ luminosity with a rather constant average energy, while in the Garching model the signal rises till $t_{\rm p.b.} \sim 0.1\,$s reflecting the rise of the $\overline{\nu}_x$ luminosity and average energy in this time window (see Fig. 1).

Given the large number of events expected in IceCube and the relatively large differences between the IH and NH case, statistical errors (also including the noise in the detectors) should not limit the capability to distinguish the two cases. The main limitation is expected to come from the systematic errors in the expectations from simulations for the two kinds of spectra: *Is it possible to discriminate between the two scenarios (IH vs. NH) independently of the simulation model?*

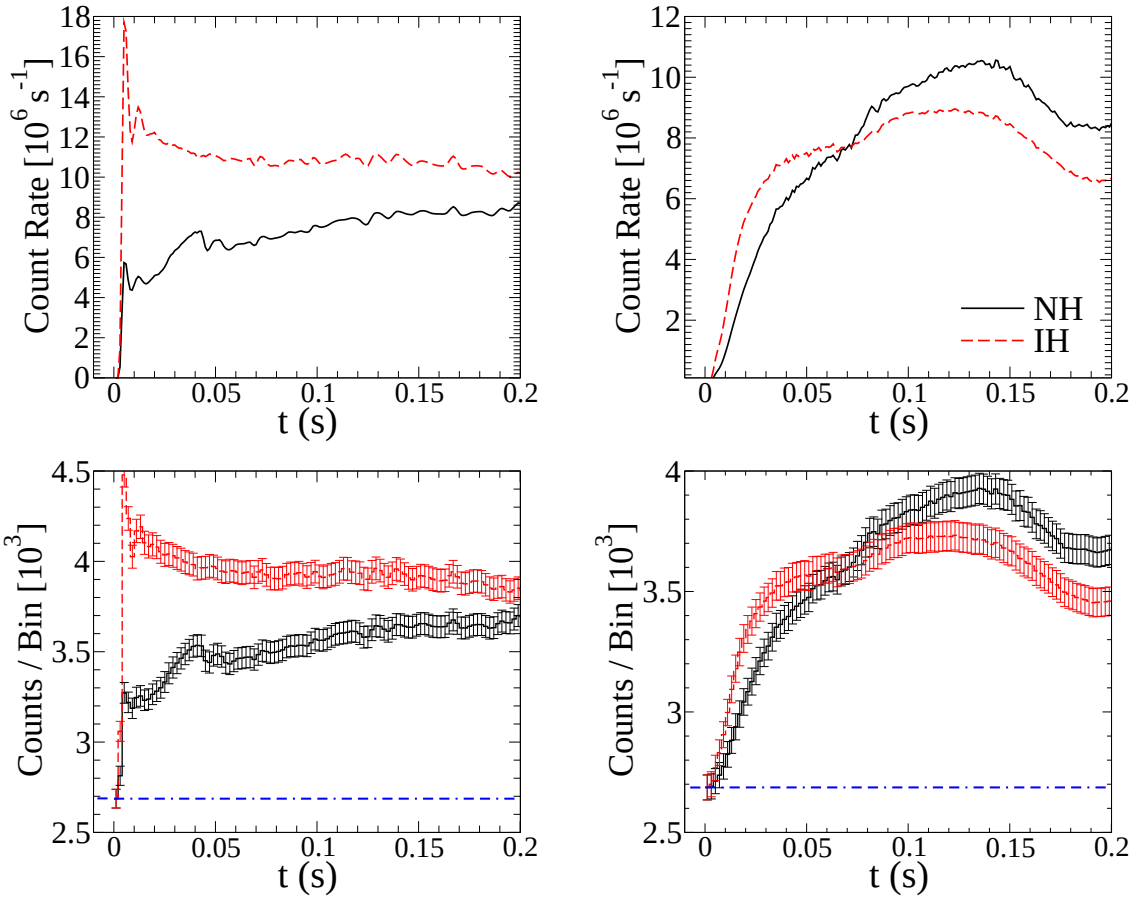

Figure 3. Supernova signal in IceCube assuming a distance of 10 kpc, based on the simulations for a 15 $M_\odot$ progenitor mass from Basel/Damstadt (left panel) and Garching (right panel) group. In bottom panels we have used 2 ms bins with typical error estimates from the photomultiplier background noise.

Although giving a definite answer to this question is beyond the scope of this very first attempt trying to address this problem in detail, some tests we did suggest encouraging perspectives. It can be illustrate via the following example of observable diagnostics. Limiting oneself to the range $t_{\rm p.b.} < 0.2$ s after bounce (note that the bounce time can be identified within 3-4 ms according to the analysis in [63]), in Table 1 we present the time needed for the IceCube signal to reach 50% of its maximum (denoted with $t_{1/2}$), and its maximum ($t_{\rm max}$) for SN models with different progenitor masses from Basel/Darmstadt and Garching groups in the two different mass hierarchies. For the Garching 15 $M_\odot$ progenitor mass we compare the rise time for a 1D and 2D model. This latter is based on Ref. [50]. The upper panel refers to the Garching models while the lower one to the Basel/Darmstadt ones. These data are represented in Fig. 4 in the plane $t_{\rm max}$ vs $t_{1/2}$. In all the models we considered, the IH cases lie inside the lower-left rectangle of the $t_{\rm max} - t_{1/2}$ plane. In some cases (Basel/Darmstadt models) the two classes of signals are well separated. In particular, even if $t_{1/2}$ is very small and close to the time resolution of the detector for both the mass hierarchies, the difference in $t_{\rm max}$ for the two mass hierarchies is striking. In other cases (Garching models) the differences are less remarkable, but still appear sufficiently far apart to suggest that an appropriate

Table 1. Rise time for the signal in IceCube for Garching and Basel/Darmstadt SN models with different progenitor masses (in $M_\odot$). It is shown the time to reach the maximum, $t_{\rm max}$, and the time to reach 50 % of the maximum, $t_{1/2}$ in both mass hierarchies. Upper table: Garching simulations. Lower table: Basel/Darmstadt simulations. The case 15.0* refers to a 2D Garching simulation based on Ref. [50].

$M_\odot$	NH	$t_{1/2}$ (s)	$t_{\rm max}$ (s)	IH	$t_{1/2}$ (s)	$t_{\rm max}$
12.0		0.027	0.171		0.0135	0.099
13.8		0.032	0.189		0.0170	0.094
15.0		0.033	0.143		0.0160	0.110
15.0*		0.033	0.153		0.0120	0.099
17.8		0.037	0.199		0.0180	0.094
20.0		0.031	0.108		0.0172	0.101
25.0		0.054	0.200		0.0225	0.105
35.0		0.039	0.193		0.0180	0.111
36.0		0.041	0.201		0.0180	0.098
40.0		0.045	0.190		0.0200	0.110

$M_\odot$	NH	$t_{1/2}$ (s)	$t_{\rm max}$ (s)	IH	$t_{1/2}$ (s)	$t_{\rm max}$
10.8		0.0055	0.190		0.0035	0.021
15.0		0.0090	0.199		0.0040	0.012
18.0		0.0090	0.181		0.0045	0.020

cut in this (or other) parameter spaces could separate the two cases. In particular, for the Garching 15 $M_\odot$ progenitor mass we compare the rise time for a 1D and a 2D simulation. The Garching 15 $M_\odot$ cases are marked with a black dot at the centre of a full (1D) or empty (2D) circle. We realize that the rise time at $t_{\rm p.b.} < 0.2$ s is only marginally affected by the dimensionality of the SN simulation, as expected from our discussion in Sec. 2. For the sample at hand, one can also conceive cuts which would lead to the correct inference on the hierarchy independently of which one of the two sets of simulations is closer to reality. It seems obvious that these kinds of rise-time observables during the accretion phase deserve further scrutiny in the light of other and forthcoming simulations.

It should also be noted that we have been comparing *on purpose* a wide variety of simulations, changing the progenitor, the physics implemented and the code: qualitatively, the faster rise time for IH vs. NH appears to be a robust feature. Also, there seems to be a weak quantitative dependence on the progenitor: we can tentatively conclude that the feature remains robust with respect to the astrophysical input. Quantitative differences remain when using the core-collapse results from different teams. In the investigated sets of models these are likely to primarily originate from the use of different progenitor stars, different nuclear equations of state, and different treatments of neutrino-matter interactions rather than from different treatments of numerical aspects like the hydrodynamics and transport methods, discretization schemes or resolution. In this sense, they should provide an overestimate of the "theoretical error", consistent with our conservative approach.

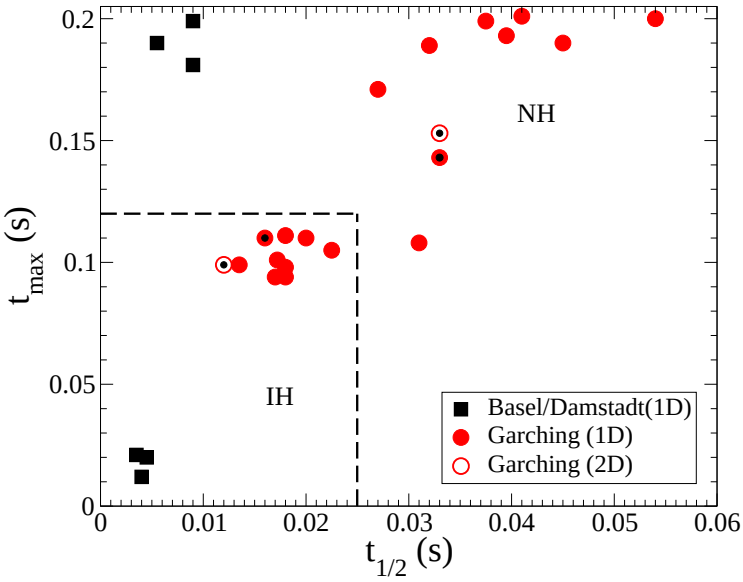

Figure 4. Rise time of the neutrino signal detection in IceCube: time to reach its maximum, $t_{\rm max}$, vs. time to get to 50% of the maximum, $t_{1/2}$. Circles correpond to Garching models, and squares to Basel/Darmstadt models with different progenitor masses (see Table 1). The Garching 15 $M_\odot$ cases are marked with a black dot at the centre of a full (1D) or empty (2D) circle. The lower-left rectangle in the plot contains IH cases, while points outside the rectangle refer to NH cases.

5 Conclusions

We explored the chances of neutrino mass-hierarchy diagnostics by the $\overline{\nu}_e$ signals during the (early) accretion phase of iron-core SNe. In particular, for the first time we have tentatively identified the rise time of the signal as a possible key observable in this context. This is a consequence of the suppression of collective oscillation effects at early postbounce times by matter multi-angle effects recently highlighted, and of the following evolution being dictated by MSW transitions. We have shown that already a current detector like IceCube should be able to measure this rise of the neutrino lightcurve sufficiently well for a typical Galactic SN to allow, in principle, to discriminate between IH and NH for not too small values of θ_{13}, provided that the *gross features* of the time profiles of the luminosity and energy are sufficiently well predicted by SN simulations.

As a first step, we have studied the variation of the signal time-profile in IceCube with respect to different progenitor masses and microphysics applied in the supernova simulations. Although some quantitative differences depend on these aspects, their origin is at least partially understood and they do not appear to prevent the separation of the two kinds of signal. In particular, we showed as an illustrative example how a cut in the $t_{\rm max}$-$t_{1/2}$ plane suggests that a rise-time and therefore hierarchy discrimination is possible. Since the feature we identified is physical (rather than numerical), it is likely that future improvements in the numerical treatments will sharpen the theoretical expectation. It also remains worth investigating optimal choices of discrimination observables, of which we introduced here a new example.

We remind the reader that the information on the mass hierarchy from the rise time of the neutrino signal in IceCube is complementary to the one that can be extracted through the Earth matter effect on SN neutrinos (see, e.g., Ref. [62]). The interesting point is that, different from the Earth effect, the signature discussed here appears to be independent of a *serendipitous* position of the detector at the arrival time of the SN signal. Also, different from shock effects, it is independent of poorly understood details of the flavor evolution in the SN during the complex cooling phase.

It is encouraging that when the next galactic SN will eventually occur, the simulations will be calibrated to reproduce that particular event. Therefore, the uncertainties discussed in the current analysis (e.g., the progenitor and the equation of state) will be significantly reduced. Additionally, if a complementary detector of ν_e's was available [30], one might hope to cross-check the preferred solution (IH or NH) from rise-time information with the inference on the hierarchy from the detection or absence of the neutronization burst [4]. This argument confirms once more the high physics potential of supernova neutrinos in shedding light on the still unknown pieces of the neutrino mass and mixing framework. Therefore, even though a galactic SN explosion is a rare event, we are sure that the patient waiting will eventually be rewarded with a bonanza of information.

Acknowledgments

We thank Ricard Tomàs for collaboration during the initial development of this project. We also thank Georg Raffelt and Irene Tamborra for reading the manuscript and for useful comments on it. L.H. and H.-T.J. are grateful to Andreas Marek and Bernhard Müller for their support. The work of S.C., A.M. was supported by the German Science Foundation (DFG) within the Collaborative Research Center 676 "Particles, Strings and the Early Universe". T.F. acknowledges support from the Swiss National Science Foundation (SNF) under grant no. PBBSP2-133378 and HIC for FAIR. At Garching, the project was partially funded by the Deutsche Forschungsgemeinschaft through the Transregional Collaborative Research Centers SFB/TR 27 "Neutrinos and Beyond" and SFB/TR 7 "Gravitational Wave Astronomy", and the Cluster of Excellence EXC 153 "Origin and Structure of the Universe" (`http://www.universe-cluster.de`). The supernova simulations were possible by computer time grants at the John von Neumann Institute for Computing (NIC) in Jülich, the Höchstleistungsrechenzentrum of the Stuttgart University (HLRS) under grant number SuperN/12758, the Leibniz-Rechenzentrum München, and the RZG in Garching.

References

[1] G. G. Raffelt, "Physics opportunities with supernova neutrinos," Prog. Part. Nucl. Phys. **64**, 393-399 (2010).

[2] S. P. Mikheev, A. Y. Smirnov, "Resonance Amplification of Oscillations in Matter and Spectroscopy of Solar Neutrinos," Sov. J. Nucl. Phys. **42**, 913-917 (1985).

[3] L. Wolfenstein, "Neutrino Oscillations in Matter," Phys. Rev. **D17**, 2369-2374 (1978).

[4] A. S. Dighe, A. Y. Smirnov, "Identifying the neutrino mass spectrum from the neutrino burst from a supernova," Phys. Rev. **D62**, 033007 (2000). [hep-ph/9907423].

[5] J. Pantaleone, "Neutrino oscillations at high densities," Phys. Lett. B **287**, 128 (1992).

[6] Y. Z. Qian and G. Fuller, "Neutrino-neutrino scattering and matter enhanced neutrino flavor transformation in Supernovae," Phys. Rev. D **51**, 1479 (1995) [astro-ph/9406073].

[7] H. Duan, G. M. Fuller, Y. -Z. Qian, "Collective Neutrino Oscillations," Ann. Rev. Nucl. Part. Sci. **60**, 569-594 (2010) [arXiv:1001.2799 [hep-ph]].

[8] H. Duan, G. M. Fuller, J. Carlson, Y. -Z. Qian, "Simulation of Coherent Non-Linear Neutrino Flavor Transformation in the Supernova Environment. 1. Correlated Neutrino Trajectories," Phys. Rev. **D74**, 105014 (2006) [astro-ph/0606616].

[9] G. L. Fogli, E. Lisi, A. Marrone, A. Mirizzi, "Collective neutrino flavor transitions in supernovae and the role of trajectory averaging," JCAP **0712**, 010 (2007) [arXiv:0707.1998 [hep-ph]].

[10] B. Dasgupta, A. Dighe, G. G. Raffelt, A. Y. .Smirnov, "Multiple Spectral Splits of Supernova Neutrinos," Phys. Rev. Lett. **103**, 051105 (2009) [arXiv:0904.3542 [hep-ph]].

[11] H. Duan, A. Friedland, "Self-induced suppression of collective neutrino oscillations in a supernova," Phys. Rev. Lett. **106**, 091101 (2011) [arXiv:1006.2359 [hep-ph]].

[12] A. Mirizzi, R. Tomas, "Multi-angle effects in self-induced oscillations for different supernova neutrino fluxes," Phys. Rev. **D84**, 033013 (2011) [arXiv:1012.1339 [hep-ph]].

[13] A. Mirizzi, P. D. Serpico, "Instability in the dense supernova neutrino gas with flavor-dependent angular distributions," [arXiv:1110.0022 [hep-ph]].

[14] S. Choubey, B. Dasgupta, A. Dighe, A. Mirizzi, "Signatures of collective and matter effects on supernova neutrinos at large detectors," [arXiv:1008.0308 [hep-ph]].

[15] R. C. Schirato, G. M. Fuller, "Connection between supernova shocks, flavor transformation, and the neutrino signal," [astro-ph/0205390].

[16] G. L. Fogli, E. Lisi, D. Montanino, A. Mirizzi, "Analysis of energy and time dependence of supernova shock effects on neutrino crossing probabilities," Phys. Rev. **D68**, 033005 (2003) [hep-ph/0304056].

[17] G. L. Fogli, E. Lisi, A. Mirizzi, D. Montanino, "Probing supernova shock waves and neutrino flavor transitions in next-generation water-Cerenkov detectors," JCAP **0504**, 002 (2005) [hep-ph/0412046].

[18] G. L. Fogli, E. Lisi, A. Mirizzi, D. Montanino, "Damping of supernova neutrino transitions in stochastic shock-wave density profiles," JCAP **0606**, 012 (2006) [hep-ph/0603033].

[19] R. Tomas, M. Kachelriess, G. Raffelt, A. Dighe, H. -T. Janka, L. Scheck, "Neutrino signatures of supernova shock and reverse shock propagation," JCAP **0409**, 015 (2004) [astro-ph/0407132].

[20] T. Fischer, S. C. Whitehouse, A. Mezzacappa, F. -K. Thielemann, M. Liebendorfer, "Protoneutron star evolution and the neutrino driven wind in general relativistic neutrino radiation hydrodynamics simulations," Astron. Astrophys. **517**, A80 (2010) [arXiv:0908.1871 [astro-ph.HE]].

[21] L. Hüdepohl, B. Müller, H. -T. Janka, A. Marek, G. G. Raffelt, "Neutrino Signal of Electron-Capture Supernovae from Core Collapse to Cooling," Phys. Rev. Lett. **104**, 251101 (2010) [arXiv:0912.0260 [astro-ph.SR]].

[22] S. Hannestad, G. G. Raffelt, G. Sigl, Y. Y. Y. Wong, "Self-induced conversion in dense neutrino gases: Pendulum in flavour space," Phys. Rev. **D74**, 105010 (2006) [astro-ph/0608695].

[23] H. Duan, G. M. Fuller, J. Carlson, Y. -Z. Qian, "Flavor Evolution of the Neutronization Neutrino Burst from an O-Ne-Mg Core-Collapse Supernova," Phys. Rev. Lett. **100**, 021101 (2008) [arXiv:0710.1271 [astro-ph]].

[24] B. Dasgupta, A. Dighe, A. Mirizzi, G. G. Raffelt, "Spectral split in prompt supernova neutrino burst: Analytic three-flavor treatment," Phys. Rev. **D77**, 113007 (2008) [arXiv:0801.1660 [hep-ph]].

[25] M. Kachelriess, R. Tomas, R. Buras, H. -T. .Janka, A. Marek, M. Rampp, "Exploiting the neutronization burst of a galactic supernova," Phys. Rev. **D71**, 063003 (2005) [astro-ph/0412082].

[26] K. Abe *et al.* [T2K Collaboration], "Indication of Electron Neutrino Appearance from an Accelerator-produced Off-axis Muon Neutrino Beam," Phys. Rev. Lett. **107**, 041801 (2011) [arXiv:1106.2822 [hep-ex]]

[27] P. Adamson *et al.* [MINOS Collaboration], "Improved search for muon-neutrino to electron-neutrino oscillations in MINOS," Phys. Rev. Lett. **107**, 181802 (2011) [arXiv:1108.0015 [hep-ex]].

[28] G. L. Fogli, E. Lisi, A. Marrone, A. Palazzo and A. M. Rotunno, "Evidence of theta(13)>0 from global neutrino data analysis," Phys. Rev. D **84**, 053007 (2011) [arXiv:1106.6028 [hep-ph]].

[29] T. Schwetz, M. Tortola and J. W. F. Valle, "Where we are on θ_{13}: addendum to 'Global neutrino data and recent reactor fluxes: status of three-flavour oscillation parameters'," New J. Phys. **13**, 109401 (2011) [arXiv:1108.1376 [hep-ph]].

[30] I. Gil Botella, A. Rubbia, "Oscillation effects on supernova neutrino rates and spectra and detection of the shock breakout in a liquid argon TPC," JCAP **0310**, 009 (2003) [hep-ph/0307244].

[31] G. Pagliaroli, F. Vissani, M. L. Costantini, A. Ianni, "Improved analysis of SN1987A antineutrino events," Astropart. Phys. **31**, 163-176 (2009) [arXiv:0810.0466 [astro-ph]].

[32] S. Chakraborty, T. Fischer, A. Mirizzi, N. Saviano, R. Tomas, "No collective neutrino flavor conversions during the supernova accretion phase," Phys. Rev. Lett. **107**, 151101 (2011) [arXiv:1104.4031 [hep-ph]].

[33] S. Chakraborty, T. Fischer, A. Mirizzi, N. Saviano, R. Tomas, "Analysis of matter suppression in collective neutrino oscillations during the supernova accretion phase," Phys. Rev. **D84**, 025002 (2011) [arXiv:1105.1130 [hep-ph].

[34] A. Esteban-Pretel, A. Mirizzi, S. Pastor, R. Tomas, G. G. Raffelt, P. D. Serpico, G. Sigl, "Role of dense matter in collective supernova neutrino transformations," Phys. Rev. **D78**, 085012 (2008) [arXiv:0807.0659 [astro-ph]].

[35] S. Sarikas and G. Raffelt, "Flavor stability analysis of supernova neutrino fluxes compared with simulations," arXiv:1110.5572 [astro-ph.SR].

[36] S. Sarikas, G. G. Raffelt, L. Hüdepohl, H. -T. Janka, "Flavor stability of a realistic accretion-phase supernova neutrino flux," [arXiv:1109.3601 [astro-ph.SR]].

[37] Results from an extended set of 1D core-collapse simulations by L. Hüdepohl for a variety of progenitors from [38] can be found at `http://www.mpa-garching.mpg.de/ccsnarchive`; results from a partially overlapping set of models were discussed in detail in Ref. [39] (see in particular Appendix B there).

[38] S. E. Woosley, S. Heger and T. A., Weaver, "The evolution and explosion of massive stars," Rev. Mod. Phys. **74**, 1015 (2002).

[39] R. Buras, H.-T. Janka, M. Rampp and K. Kifonidis, "Two-Dimensional Hydrodynamic Core-Collapse Supernova Simulations with Spectral Neutrino Transport II. Models for Different Progenitor Stars," Astron. Astrophys. **457**, 281-308 (2006) [astro-ph/0512189].

[40] M. Liebendörfer, O. E. B. Messer, A. Mezzacappa, S. W. Bruenn, C. Y. Cardall and F. K. Thielemann, "A finite difference representation of neutrino radiation hydrodynamics for spherically symmetric general relativistic supernova simulations," Astrophys. J. Suppl. **150**, 263 (2004).

[41] S. W. Bruenn, "Stellar core collapse: Numerical model and infall epoch," Astrophys. J. Suppl. **58**, 771 (1985).

[42] S. Hannestad and J. Madsen, "Supernova neutrino opacity from nucleon-nucleon Bremsstrahlung and related processes," Phys. Rev. D **507**, 339 (1998).

[43] H. Shen, H. Toki, K. Oyamatrsu and K. Sumiyoshi, "Relativistic equation of state of nuclear matter for supernova and neutron star," Nucl. Phys. **A637**, 435 (1998).

[44] M. Rampp and H.-Th. Janka, "Radiation hydrodynamics with neutrinos: Variable Eddington factor method for core-collapse supernova simulations," Astron. Astrophys. **396**, 361 (2002). [astro-ph/0203101].

[45] R. Buras *et al.*, "Two-dimensional hydrodynamic core-collapse supernova simulations with spectral neutrino transport. I. Numerical method and results for a 15 M_{sun} star," Astron. Astrophys. **447**, 1049 (2006). [astro-ph/0507135].

[46] A. Marek *et al.*, "Exploring the relativistic regime with Newtonian hydrodynamics: an improved effective gravitational potential for supernova simulations," Astron. Astrophys. **445**, 273 (2006). [astro-ph/0502161].

[47] K. Langanke *et al.*, "Electron capture rates on nuclei and implications for stellar core collapse," Phys. Rev. Lett. **90**, 241102 (2003). [astro-ph/0302459].

[48] K. Langanke *et al.*, "Effects of Inelastic Neutrino-Nucleus Scattering on Supernova Dynamics and Radiated Neutrino Spectra," Phys. Rev. Lett. **100**, 011101 (2008). [arXiv:0706.1687 [astro-ph]].

[49] S. E. Woosley and T. A Weaver, "The Evolution and explosion of massive stars. 2. Explosive hydrodynamics and nucleosynthesis" Astrophys. J. Suppl. **101**, 181 (1995).

[50] A. Marek, H. T. Janka and E. Müller, "Equation-of-State Dependent Features in Shock-Oscillation Modulated Neutrino and Gravitational-Wave Signals from Supernovae," Astron. Astrophys. **496**, 475 (2009). [arXiv:0808.4136 [astro-ph]].

[51] J. M. Lattimer and F. D. Swesty, "A generalized equation of state for hot, dense matter," Nucl. Phys. A **535**, 331 (1991).

[52] M. Liebendörfer, M. Rampp, H.-Th. Janka and A. Mezzacappa, "Supernova Simulations with Boltzmann Neutrino Transport: A Comparison of Methods," Astrophys. J. **620**, 840 (2005) [astro-ph/0310662].

[53] M. T. Keil, G. G. Raffelt and H. T. Janka, "Monte Carlo study of supernova neutrino spectra formation," Astrophys. J. **590**, 971 (2003) [astro-ph/0208035].

[54] B. Müller, H.-Th. Janka and H. Dimmelmeier, "A new multi-dimensional general relativistic neutrino hydrodynamics code for core-collapse supernovae. I. Method and code tests in spherical symmetry," Astrophys. J. Suppl. **189**, 104 (2010) [arXiv:1001.4841 [astro-ph.SR]].

[55] G. G. Raffelt, "Mu- and tau-neutrino spectra formation in supernovae," Astrophys. J. **561**, 890 (2001) [astro-ph/0105250].

[56] C. D. Ott, A. Burrows, L. Dessart and E. Livne, "2D Multi-Angle, Multi-Group Neutrino Radiation-Hydrodynamic Simulations of Postbounce Supernova Cores," Astrophys. J. **685**, 1069 (2008) [arXiv:0804.0239 [astro-ph]].

[57] E. Müller, H. T. Janka and A. Wongwathanarat, "Parametrized 3D models of neutrino-driven supernova explosions: Neutrino emission asymmetries and gravitational-wave signals," arXiv:1106.6301 [astro-ph.SR].

[58] B. Dasgupta, E. P. O'Connor, and C. D. Ott, "The Role of Collective Neutrino Flavor Oscillations in Core-Collapse Supernova Shock Revival," [arXiv:1106.1167 [astro-ph.SR]]

[59] F. Halzen, J. E. Jacobsen, E. Zas, "Possibility that high-energy neutrino telescopes could

detect supernovae," Phys. Rev. **D49**, 1758 (1994).

[60] R. Abbasi *et al.* [IceCube Collaboration], "IceCube Sensitivity for Low-Energy Neutrinos from Nearby Supernovae," [arXiv:1108.0171 [astro-ph.HE]].

[61] A. Strumia, F. Vissani, "Precise quasielastic neutrino/nucleon cross-section," Phys. Lett. **B564**, 42-54 (2003) [astro-ph/0302055].

[62] A. S. Dighe, M. T. Keil and G. G. Raffelt, "Detecting the neutrino mass hierarchy with a supernova at IceCube," JCAP **0306**, 005 (2003) [hep-ph/0303210].

[63] F. Halzen, G. G. Raffelt, "Reconstructing the supernova bounce time with neutrinos in IceCube," Phys. Rev. **D80**, 087301 (2009) [arXiv:0908.2317 [astro-ph.HE]].

[64] A. Mirizzi, G. G. Raffelt, P. D. Serpico, "Earth matter effects in supernova neutrinos: Optimal detector locations," JCAP **0605**, 012 (2006) [astro-ph/0604300].